Check for updates

AGU ADVANCING EARTH AND SPACE SCIENCES

Geophysical Research Letters

RESEARCH LETTER
10.1029/2023GL105626

Lidar Observations of Predawn Thermosphere-Ionosphere Na (TINa) Layers Over Boulder (40.13°N, 105.24°W): Annual Phase Variations and Correlation With Sunrise and Tidal Winds

Yingfei Chen[1] and **Xinzhao Chu**[1]

[1]Cooperative Institute of Research in Environmental Sciences & Department of Aerospace Engineering Sciences, University of Colorado Boulder, Boulder, CO, USA

Key Points:

- First characterization of 12 monthly composites of Na mixing ratios reveals annual phase variations of predawn thermosphere-ionosphere Na (TINa) layers (110–150 km)
- Predawn TINa occur ∼2.5 hr earlier in summer than in winter, closely correlating to annual phase variations of sunrise and Climatological Tidal Model of the Thermosphere semidiurnal westward-propagating tidal winds
- TINa layers descend at similar rates as and in tidal-wind-modeled ion convergence regions, supporting neutralization of $TINa^+$ forming TINa

Supporting Information:

Supporting Information may be found in the online version of this article.

Correspondence to:

X. Chu,
Xinzhao.Chu@Colorado.edu

Citation:

Chen, Y., & Chu, X. (2023). Lidar observations of predawn thermosphere-ionosphere Na (TINa) layers over Boulder (40.13°N, 105.24°W): Annual phase variations and correlation with sunrise and tidal winds. *Geophysical Research Letters*, *50*, e2023GL105626. https://doi.org/10.1029/2023GL105626

Received 23 JUL 2023
Accepted 27 AUG 2023

Author Contributions:

Conceptualization: Xinzhao Chu
Data curation: Xinzhao Chu
Formal analysis: Yingfei Chen, Xinzhao Chu
Funding acquisition: Xinzhao Chu
Investigation: Yingfei Chen, Xinzhao Chu
Methodology: Yingfei Chen, Xinzhao Chu

© 2023. The Authors.
This is an open access article under the terms of the Creative Commons Attribution-NonCommercial-NoDerivs License, which permits use and distribution in any medium, provided the original work is properly cited, the use is non-commercial and no modifications or adaptations are made.

Abstract We have discovered that the peak phase time of predawn thermosphere-ionosphere Na (TINa) layers (∼110–150 km altitude) undergoes clear annual variations with the earliest occurrence in summer and latest in winter over Boulder (40.13°N, 105.24°W), which are closely correlated to annual phase variations of sunrise and tidal winds. Such discoveries were enabled by the first characterization of 12 monthly composites of TINa layers from January through December using 7 years of lidar observations (2011–2017). Despite their tenuous densities, the predawn TINa layers have nearly 100% occurrence rate (160 out of 164 nights of observations). Monthly composites show downward-phase-progression TINa descending at similar phase speeds as Climatological Tidal Model of the Thermosphere tidal winds. These TINa layers occur in ion convergence but neutral divergence regions, modeled using tidal winds. These results support the formation mechanism (neutralization of converged $TINa^+$ forming TINa) proposed previously and suggest that migrating tidal winds experience annual phase variations.

Plain Language Summary With tons of cosmic dust falling on Earth every day, metallic atoms and ions (e.g., Fe, Na, K, and Ca^+) are released via meteor ablation and sputtering into the upper atmosphere, forming permanent metal layers (∼75–105 km) that have been known for nearly a century. What was unknown until 2011 was the existence of thermosphere-ionosphere metal (TIMt) layers that were discovered with high-sensitivity lidar observations first from Antarctica and then were observed globally. These neutral TIMt layers locate above the permanent layers with an upper reach to ∼200 km and exhibit intermittent occurrence. In 2021 surprising regular occurrence of TIMt layers in Na species (TINa) was reported for the first time from lidar observations over Boulder, Colorado, where TINa layers occur before dawn and after dusk nearly every night. By analyzing 7 years of lidar data, we have further discovered that the Boulder predawn TINa layers occur in earlier hours in summer than in winter. Such annual phase variations are correlated with sunrise and solar-heating-driven tidal winds. These TIMt layers are of great scientific interest as they provide unique tracers for making direct measurements in the least understood but crucially important "thermospheric gap" region of 100–200 km.

1. Introduction

Since the first discovery of thermosphere-ionosphere metal (TIMt) layers by lidar observations in Antarctica (Chu et al., 2011), TIMt layers have been reported in Fe (TIFe), Na (TINa), and K (TIK) in the 100–200 km altitudes and in Ca^+ ($TICa^+$) up to 300 km with intermittent occurrence in the polar regions (e.g., Chu et al., 2011, 2020; Lübken et al., 2011; Tsuda et al., 2015) and at mid-to-low latitudes (e.g., Friedman et al., 2013; Gao et al., 2015; Jiao et al., 2022; Liu et al., 2016; Raizada et al., 2015, 2020; Smith & Chu, 2015; Wang et al., 2012; Xun et al., 2019). In stark contrast to the intermittent occurrence, high-sensitivity Na Doppler lidar observations at Boulder have revealed the regular occurrence of TINa layers in the 100–200 km (Chu et al., 2021). These Boulder TINa layers occur regularly after dusk and before dawn in all six cases reported in that paper and tens of other cases examined at that time. Both post-dusk and predawn layers show downward-progression phases in the Na mixing ratio contours, consistent with the semidiurnal tidal wind phases over Boulder, according to Hough-Mode-Extension (HME) tidal winds measured by the Ionospheric Connection Explorer (ICON) (Chu et al., 2021; Cullens et al., 2020; Immel et al., 2018).

19448007, 2023, 18, Downloaded from https://agupubs.onlinelibrary.wiley.com/doi/10.1029/2023GL105626, Wiley Online Library on [13/09/2023]. See the Terms and Conditions (https://onlinelibrary.wiley.com/terms-and-conditions) on Wiley Online Library for rules of use; OA articles are governed by the applicable Creative Commons License

Project Administration: Xinzhao Chu
Resources: Xinzhao Chu
Software: Yingfei Chen, Xinzhao Chu
Supervision: Xinzhao Chu
Validation: Yingfei Chen, Xinzhao Chu
Visualization: Yingfei Chen
Writing – original draft: Xinzhao Chu
Writing – review & editing: Yingfei Chen, Xinzhao Chu

There are compelling reasons to study TIMt layers. First, these metal layers provide a natural laboratory for studying the mechanisms of ion transport and plasma-neutral coupling in the E–F regions, as leading theories hypothesize that neutral TIMt layers are formed via the neutralization of converged TIMt$^+$ ion layers (e.g., Chu & Yu, 2017; Chu et al., 2011, 2020, 2021; Plane et al., 2015). Second, these layers provide unique tracers for profiling temperatures and winds in the E to F regions (~100–300 km), helping fill the "thermospheric gap" (Forbes et al., 2022; Oberheide et al., 2011). While significant efforts have been spent on closing this gap, many of these methods use indirect techniques, for example, HME modeling is widely used to extend observations from the mesopause region into the middle/upper thermosphere. In contrast, lidar detections of TIMt and TIMt$^+$ layers between 100 and 300 km offer direct measurements of neutral species, metallic ions, temperatures, and neutral winds in this "thermospheric gap" region, which will help study the "space weather" of the thermosphere and ionosphere (Oberheide, 2022).

Of particular interest are the TINa layers with regular occurrence (Chu et al., 2021) as they provide a new tracer to delineate thermospheric tides in this gap region. This study utilizes 7-year lidar data (2011–2017) from Boulder to explore the predawn TINa layers and their relation to tidal winds. Not only do we provide the first-ever characterization of 12 monthly composites of TIMt layers, but we also discover the predawn TINa layer phase varying with season and correlating well with sunrise time. Researching the possible causes, we find from the Climatological Tidal Model of the Thermosphere (CTMT) (Oberheide et al., 2011) that the phases of semidiurnal westward-propagating tidal winds (SW2) undergo similar annual variations as sunrise and predawn TINa. Such TIMt studies provide clues for the TIMt formation mechanisms and a new perspective to investigate thermal tides.

2. First Characterization of 12 Monthly Composites of Boulder Predawn TINa Layers

The lidar observations, which led to the discovery of TINa regular occurrence, were made from 2011 to 2017 at Table Mountain Observatory (40.13°N, 105.24°W), north Boulder, Colorado. Such high-sensitivity detection of tenuous TINa layers was enabled by the advanced Na Doppler lidar technologies as described in Smith and Chu (2015) and Chu et al. (2021). The raw photon counts were collected in temporal and vertical resolutions of 3 s and 24 m. To achieve sufficient signal-to-noise ratios (SNRs), all data of Na densities, temperatures, and vertical winds were retrieved with the same temporal integration of 7.5 min and spatial binning of 960 m. Na mixing ratios are then calculated by dividing Na densities with the corresponding total number densities of the atmosphere computed from MSISE00 (Picone et al., 2002).

Through 7 years of lidar observations, totally 225 nights of data were accumulated. Only 164 nights were chosen for predawn TINa examination. Because the time separation between TINa peak phase and sunrise can exceed 2 hr, only data duration longer than 3 hr and covering sunrise are included. Another screening criterion is that data must possess sufficiently high SNRs which are necessary for identifying these tenuous layers. In the Na mixing ratio contours of qualified nights, predawn TINa layers are identified as layer structures that possess continuous phase evolutions of peak Na mixing ratios and whose maximum peak altitudes reach above 125 km. This threshold of 125 km is chosen to distinguish TINa layers from sporadic metal layers in the altitude range of 80–105 km (Plane, 2003) and from thermosphere-ionosphere sporadic metal layers (Wu et al., 2022) that are usually below 120 km. Meteoric ablation efficiency decreases significantly above this altitude (Plane et al., 2015).

Predawn TINa layers were found in 160 nights out of the 164 qualified nights. Each of the 160 nights shows a single predawn TINa layer, exhibiting clear downward phase progression, similar to the six cases shown in Chu et al. (2021). Figure S1 in Supporting Information S1 shows 12 more examples from January through December. The monthly distributions of the qualified nights and predawn TINa nights are listed in Table S1 in Supporting Information S1. The occurrence rates are 100% in January–March and July–December, regardless of the number of monthly observations ranging from 5 to 30 nights. Only 4 nights in April to June did not show predawn TINa layers, likely related to geomagnetic disturbance. These four cases are beyond the scope of this paper but will be addressed in future studies. The overall occurrence rate of Boulder predawn TINa is 97.56%. Such nearly 100% occurrence rate has unequivocally confirmed the surprisingly regular occurrence of TINa layers over Boulder discovered by Chu et al. (2021).

Among the 160 cases, predawn TINa appear around similar time and descend from similar altitudes within the same month but exhibit different features among different months. For instance, most TINa cases in November start around 10 UT and descend from 140 to 110 km with phase speeds of ~2.7 m/s, similar to the three

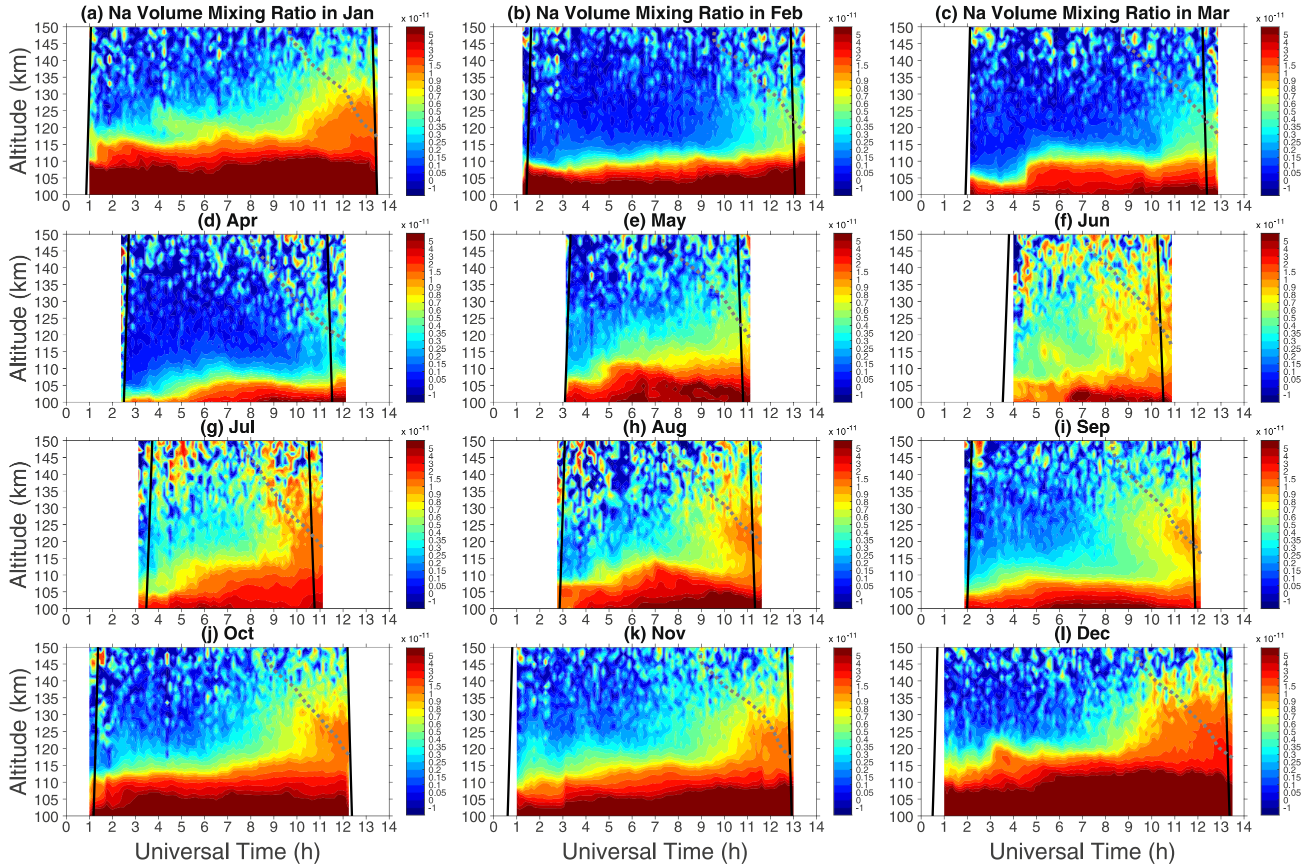

Figure 1. 12 monthly composite contours of Na mixing ratios of predawn TINa layers from January through December over Boulder. The black lines in each panel represent the minimum sunlit altitudes at sunset on the left and at sunrise on the right. The dotted-gray lines track the TINa peak phases. 7 UT is the local midnight.

cases shown in Chu et al. (2021), but the predawn TINa layers start earlier in summer than in winter (Figure S1 in Supporting Information S1). To characterize the similarities within the same month but the differences among different months, taking the monthly composites from January to December is a viable solution because monthly composites largely reduce incoherent features while preserving coherent structures within each month.

To form monthly composites, the 160 TINa nights are further screened. Eventually 138 nights are used in monthly composites (see the monthly distribution in Table S1 in Supporting Information S1) after excluding data with gaps. June has the least but still four cases, sufficient for composite calculations, while maximum 24 nights of data remain in November after six nights were excluded. A monthly composite of lidar data covering from dusk to dawn is obtained by averaging TINa mixing ratios or number densities in the same local time at the same altitude bin but in different nights within the same month. Such 12 monthly-composite mixing ratio contours from January through December are plotted in Figure 1 with identical uneven color bars.

Figure 1 shows elevated Na mixing ratios in the predawn hours of all 12 months from nearly 150 to ~120 km or lower, when compared to earlier hours in the night. These elevated Na mixing ratios exhibit continuous downward phase progression from the top altitudes (roughly 135–150 km) to ~110 km in each month, and such features qualify them as the predawn TINa layers. Using the composite contour of September as an example, the downward phase of predawn TINa starts around 145 km at ~8 UT, then descends to around 115 km at ~12 UT. Such clear phase progression is stunning, especially considering the composite was made from averaging 11 nights of data taken in three different years (2013–2015). An implication is that the driving factors of these predawn TINa layers must have excellent year-to-year repeatability. Furthermore, the November and January composite contours show that the predawn layers start ~10–11 UT at ~140 km and descend to merge with the main layer ~110 km, which is comparable to the six individual cases shown in Chu et al. (2021). When we average 24 nights of data from 2011 to 2016 and 18 nights from 2013 to 2015 to make the November and Janu-

19448007, 2023, 18, Downloaded from https://agupubs.onlinelibrary.wiley.com/doi/10.1029/2023GL105626, Wiley Online Library on [13/09/2023]. See the Terms and Conditions (https://onlinelibrary.wiley.com/terms-and-conditions) on Wiley Online Library for rules of use; OA articles are governed by the applicable Creative Commons License

ary composites, respectively, incoherent features have been largely eliminated while coherent phase features remain. Therefore, these monthly composites showing predawn TINa layers indicate that the phase of the main causative agent, likely the semidiurnal tides, is not random but relatively steady from day-to-day at Boulder within each of the 12 months from January through December. We term this phenomenon as the "day-to-day phase coherence."

Now if we compare different months in Figure 1, the occurrence time of predawn TINa apparently shifts with seasons. For example, from June to December in the third column, the TINa layers occur earliest in June, later in September, and latest in December, while the occurrence in March is comparable to September but slightly later. These time shifts are likely linked to the local sunrise time varying with season, which will be investigated next.

3. Discovery of Annual Phase Variations of Predawn TINa and Correlation to Sunrise

To investigate the relation between predawn TINa occurrence and sunrise, we calculate the minimum sunlit altitude (i.e., the lowest altitude that sunlight can reach at a given solar elevation angle) for every day in one single year following the method outlined in Yu et al. (2012). After taking the individual monthly average of these altitudes from 100 to 150 km, we plot them as the black lines in Figure 1. The shift of sunrise time, which is earliest in June and latest in December, is clearly seen in the third column, following the same trend of TINa occurrence. The predawn TINa occurrence is defined as the time corresponding to maximum TINa mixing ratios, that is, the layer peak phase. To quantitatively determine the peak phase, the Na mixing ratios are smoothed with 2D Hamming windows with full widths of 0.5 hr and 5 km for minimizing noise thus better determination of the peak mixing ratios. Through identifying the proper peaks of mixing ratios, the TINa peak phase is tracked continuously from low to high altitudes and shown as dotted-gray lines in Figure 1 for readability. Figure 2a displays the September contour for detailed examination. The corresponding phase uncertainty derived from the standard deviation of various nights and the Na mixing-ratio and density profiles averaged from 9 to 12 UT are illustrated in Figures 2b–2d, respectively. Interestingly, the Na mixing ratios and number densities and their profile shapes are very similar to those published in Chu et al. (2021), for example, $\sim$1 cm^{-3} at 130 km. The peak phases of 12 monthly composites are plotted as cyan circles in Figures 2e–2h for altitudes of 135, 130, 125, and 120 km, respectively, and the corresponding local sunrise time is plotted as red circles.

Both the TINa occurrence and sunrise times exhibit obvious annual variations in Figure 2 despite some fluctuations. We apply harmonic fits given in Equation 1 to quantify the variations and derive the annual-oscillation (AO) amplitudes A_{12} and phases φ_{12} of both:

$$y = A_0 + A_{12}\cos\left[\frac{2\pi}{365}(\text{day-}\varphi_{12})\right] \tag{1}$$

The fitting coefficients are listed in Table S2 in Supporting Information S1, and the fitted curves are plotted as solid blue and red lines, respectively, for TINa peak phase and sunrise in Figures 2e–2h. The AO amplitudes of TINa and sunrise are $\sim$1.2 and $\sim$1.4 hr, respectively. The AO phases of sunrise and TINa are latest around late December to early January.

Figure 2 demonstrates that the annual variations of TINa peak phase and sunrise times are strikingly similar as they share the same trend—earliest in summer and latest in winter. Correlation coefficients between the TINa peak phase and sunrise are above 96% before fitting and above 98% after the fitting with all confidence levels nearly 100% (see Table S3 in Supporting Information S1); therefore, the TINa peak phase is positively correlated to sunrise. The time differences between winter (December/January) and summer (June/July) are $\sim$2.5 hr for TINa and $\sim$2.8 hr for sunrise. Meanwhile, the time difference between sunrise time and TINa peak phase is altitude dependent. The annual mean of such time difference is $\sim$1–2 hr at higher altitudes, and then decreases to $-$0.3 hr at 120 km. This result may be explained by the downward phase progression of TINa layers being slower than sunrise. The predawn TINa start earlier than sunrise at higher altitudes, then descend with smaller phase speeds than sunrise to lower altitudes. The TINa phase lines intersect the sunrise lines and start to lag behind sunrise around 120 km (see Figure 1).

19448007, 2023, 18, Downloaded from https://agupubs.onlinelibrary.wiley.com/doi/10.1029/2023GL105626, Wiley Online Library on [13/09/2023]. See the Terms and Conditions (https://onlinelibrary.wiley.com/terms-and-conditions) on Wiley Online Library for rules of use; OA articles are governed by the applicable Creative Commons License

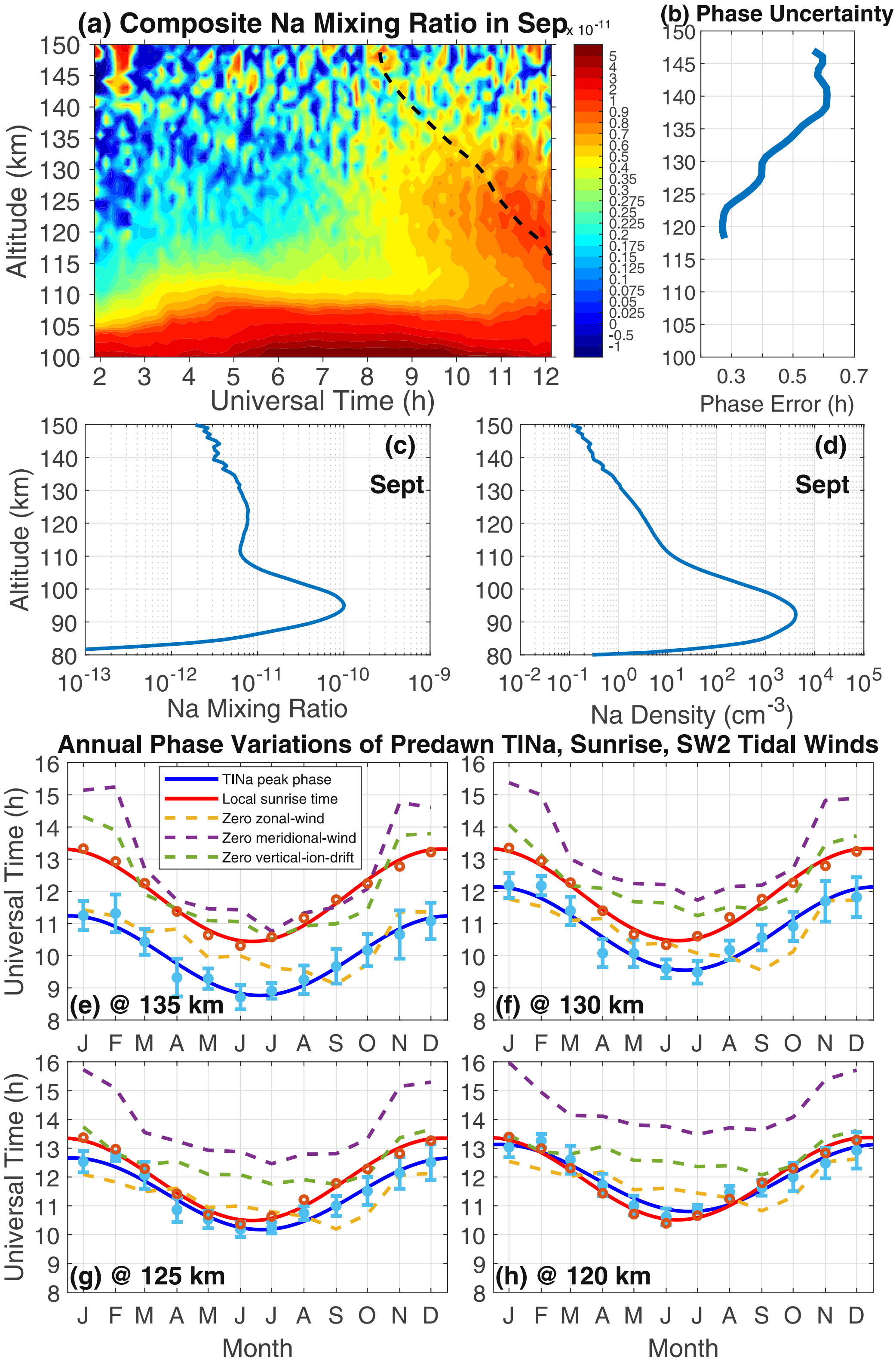

Figure 2. (a) Peak phase tracking of predawn TINa layer in September. (b) Uncertainty of the peak phase. (c–d) The altitude profiles of predawn TINa mixing ratio and density in September monthly composite. (e–h) Predawn-TINa-layer peak phase (cyan circles) and Boulder local sunrise time (red circles) from January through December at four altitudes of 135, 130, 125, and 120 km. The solid curves are the annual oscillation fittings to sunrise and TINa peak phases. Dashed lines overplotted are the phases of zero-wind lines in zonal and meridional winds and of zero vertical-ion-drift line, driven by CTMT tidal component SW2 only, which correspond to vertical ion convergence.

19448007, 2023, 18, Downloaded from https://agupubs.onlinelibrary.wiley.com/doi/10.1029/2023GL105626, Wiley Online Library on [13/09/2023]. See the Terms and Conditions (https://onlinelibrary.wiley.com/terms-and-conditions) on Wiley Online Library for rules of use; OA articles are governed by the applicable Creative Commons License

4. Correlation of Predawn TINa Layers to Tidal Winds

Important implications from the results above are that the mechanisms driving the formation and annual variation of predawn TINa layers must possess the following features: (a) "Day-to-day phase coherence" as defined earlier, (b) year-to-year repeatability, and (c) natural annual variations correlating with sunrise time. The most likely driving factor would be the tidal winds in the thermosphere as migrating tides would have good "day-to-day coherence" and year-to-year repeatability. If so, our results suggest that migrating tidal phases over Boulder should have similar annual phase variations likely driven by annual changes of solar heating. To test this hypothesis, we analyze the CTMT data (Oberheide et al., 2011) to examine over Boulder the tidal winds, annual variations, and their relation to TINa layers via $TINa^+$ ion layers.

Plotted in Figures 3a–3c are the tidal amplitude comparisons of zonal, meridional, and vertical winds given by CTMT for September over 40ºN. As SW2 and DW1 are the dominant tidal components in horizontal winds, we use their amplitudes and phases to construct the tidal zonal, meridional, and vertical winds over Boulder that are plotted in Figures 3d–3f. In the first report of Boulder TINa, Chu et al. (2021) proposed a formation mechanism—the neutralization of converged $TINa^+$ ions via recombination with electrons produces the observed neutral TINa layers ($TINa^+ + e^- \rightarrow TINa + h\nu$). $TINa^+$ ions can be accumulated in descending and ascending phases as well as in convergent wind shear (see Figure 3f in Chu et al. (2021)). To examine this hypothesis, we compute the vertical drift velocity of $TINa^+$ ions, V_{izw}, induced by tidal neutral winds in zonal ($V_{n,x}$), meridional ($V_{n,y}$), and vertical ($V_{n,z}$) directions, using the same equation and same ratio (ξ) as in Chu et al. (2021).

$$V_{izw} = \frac{\xi \cos\theta_D}{1+\xi^2} V_{n,x} - \frac{\sin(2\theta_D)}{2(1+\xi^2)} V_{n,y} + \left(1 - \frac{\cos^2\theta_D}{1+\xi^2}\right) V_{n,z} \tag{2}$$

where $\xi = \nu_{in}/\omega_i$ is the ratio of ion-neutral collision frequency (ν_{in}) to the gyro frequency (ω_i) of $TINa^+$. Here $\theta_D = 66.55°$ is the dip angle for Boulder. The vertical ion divergence ($\partial V_{izw}/\partial z$), defined as the vertical gradient of the vertical ion drift velocity (e.g., Shinagawa et al., 2017), is also computed. The results of V_{izw} and $\partial V_{izw}/\partial z$ for September are plotted in Figures 3g and 3h. The white circles overplotted on Figures 3d–3h are the TINa peak phases in September.

Interestingly, the TINa peak phases descend along the tidal wind phase lines and lie closely to the vertical shears of zonal, meridional, and vertical winds in September (Figures 3d–3f). Because eastward and southward (westward and northward) winds transport ions upward (downward) (e.g., Carter & Forbes, 1999; Chu & Yu, 2017; Chu et al., 2021), these shears of horizontal and vertical winds cause ions to converge and diverge, respectively. Because the vertical wind magnitudes are much smaller than the horizontal winds, the overall effects are ion convergence, that is, the vertical ion drift velocities are downward (upward) above (below) the TINa peak phases (Figure 3g). The occurrence region of predawn TINa layer corresponds where vertical ion divergence is negative (Figure 3h), that is, the region where $TINa^+$ ions converge to increase concentrations. Note that the zonal and meridional wind shears cannot accumulate neutrals while the vertical wind shown in Figure 3f causes neutrals to diverge at the TINa peak phases. However, this divergence, $\partial w/\partial z$, is so small (maximum ~0.1 m/s change over 15 km) that it would produce at most a few percent change in TINa density over 2 hr, that is, $\int \frac{\partial N/\partial t}{N} dt \approx \int (-\partial w/\partial z) dt \approx -4.8\%$. Similar calculations are exercised in other months using CTMT tidal winds (not shown). The TINa peak phases fall in the vertical ion convergence regions, that is, $\frac{\partial V_{izw}}{\partial z} < 0$ but on the divergent phases of neutral vertical winds in March through November, comparable to September. However, in three winter months (December–February), the CTMT meridional winds have abnormal phases below ~140 km, causing some wiggling in V_{izw} contours. Consequently, the regions where TINa layers lie have $\frac{\partial V_{izw}}{\partial z} > 0$. In contrast, when plotting the January TINa phases onto the published V_{izw} contour in January calculated with ICON HME tidal winds in Chu et al. (2021), the TINa peak phases lie in the vertical ion convergence region where $\frac{\partial V_{izw}}{\partial z} < 0$ (see Figure S3 in Supporting Information S1 for CTMT and ICON comparison in January). These results indicate that CTMT still has room to improve, especially in winter.

Nevertheless, the CTMT SW2 phases of meridional and zonal winds exhibit annual variations—the earliest in summer and latest in winter with a winter-summer difference of ~2–4 hr. We illustrate in Figures 2e–2h as dashed lines the phases of zero zonal and meridional winds of SW2 and of zero vertical-ion-drift line driven by SW2 only, corresponding to vertical ion convergence, which largely resemble the annual variation trend of TINa

19448007, 2023, 18, Downloaded from https://agupubs.onlinelibrary.wiley.com/doi/10.1029/2023GL105626, Wiley Online Library on [13/09/2023]. See the Terms and Conditions (https://onlinelibrary.wiley.com/terms-and-conditions) on Wiley Online Library for rules of use; OA articles are governed by the applicable Creative Commons License

19448007, 2023, 18, Downloaded from https://agupubs.onlinelibrary.wiley.com/doi/10.1029/2023GL105626, Wiley Online Library on [13/09/2023]. See the Terms and Conditions (https://onlinelibrary.wiley.com/terms-and-conditions) on Wiley Online Library for rules of use; OA articles are governed by the applicable Creative Commons License

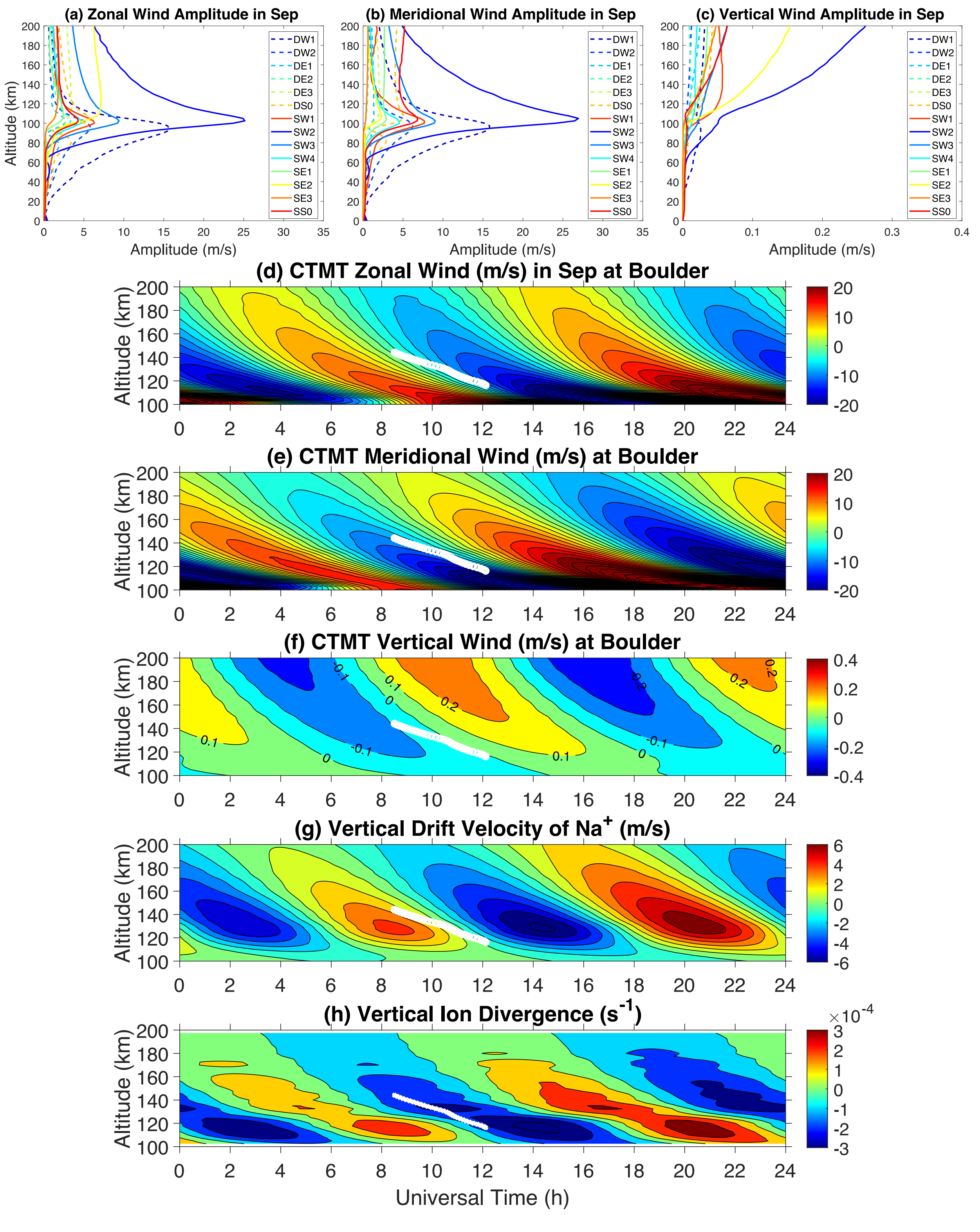

Figure 3. Comparisons of CTMT tidal amplitudes in (a) zonal, (b) meridional, and (c) vertical winds in September. (d) Zonal, (e) meridional, and (f) vertical winds reconstructed with SW2 and DW1 tidal components in September. (g) Vertical drift velocity (V_{izw}) of TINa$^+$ ions computed with the three wind components given above. (h) Vertical ion divergence ($\partial V_{izw}/\partial z$) computed from the vertical drift velocity in September. TINa peak phases are overplotted as white circles in all contours. Note that winds and velocities are positive in eastward, northward, and upward directions.

10.1029/2023GL105626

phases. The correlation coefficients between TINa and SW2 phases range from ∼0.68 to 0.94 with all confidence levels above 98% (see Table S3 in Supporting Information S1). Other tidal components like DW1 also exhibit phase variations (not shown) but somewhat different than the TINa phases. The lower-thermosphere migrating tides in CTMT include only tides propagating upward from lower-atmosphere sources (Oberheide et al., 2011), and have annual phase variations. These results suggest that the SW2 tidal winds play the major role in $TINa^+$ ion convergence thus strongly influencing the phase variations of predawn TINa layers over Boulder.

5. Discussion

The reaction rate coefficient for $TINa^+ + e^- \rightarrow TINa + h\nu$ is $k = 1.7 \times 10^{-12}$ cm^3 s^{-1} (Verner & Ferland, 1996). The production rate of TINa is $k[Na^+][e^-]$ (Chu et al., 2020; Plane et al., 2015), where $[Na^+]$ and $[e^-]$ are Na^+ and electron densities. Rocket measurements show $[Na^+]$ occupying the total electron density $\left[Na^+\right]/[e^-] = 7.41 \times 10^{-2}/1.77 = 4.18 \times 10^{-2}$ (Kopp, 1997; Wu et al., 2022). Assuming $[e^-]$ ∼5×10^4 cm^{-3} which is reasonable in converged ion layers, $[Na^+] = 5 \times 10^4 \times 4.18 \times 10^{-2} = 2.1 \times 10^3$ cm^{-3}. Thus, the production rate $k[Na^+][e^-] = 1.78 \times 10^{-4}$ cm^{-3} s^{-1}. Given 2-hr accumulation (see Figure 2a), the Na density will reach $[Na] = 1.78 \times 10^{-4}$ cm^{-3}s^{-1} $\times$ 3600 s $\times$ 2 = 1.28 cm^{-3}, higher than the Na density (∼1 cm^{-3}) observed by lidar at 130 km (Figure 2d). Considering Na loss, the numbers estimated above are reasonable and support our hypothesis.

The descending rate of TINa layer with time agrees well with the simple $TINa^+$ model based on the CTMT tidal winds (Figure 3), but some phase discrepancy exists. As ion accumulation is an integration process, the maximum $[TINa^+]$ density would occur approximately when convergence changes to divergence, ∼3 hr later. Because the conversion from TINa $^+$ to TINa is slow, the TINa maximum should occur even later. Such phase discrepancy may be related not only to possible inaccuracy of CTMT at the Boulder location, but also to three other important factors that are not considered in the simple model—the ionospheric electric fields, the mean background winds, and the in situ generated tides.

As discussed in Chu et al. (2021), the climatology of F-region ion transport at Millstone Hill (Buonsanto & Witasse, 1999; Buonsanto et al., 1993) shows in general upward ion transport in the predawn morning hours for all seasons. Assuming the Boulder E-region electric fields equal the Millstone Hill F-region values, the ion drift velocities below 150 km depart from their F-region values due to ion-neutral collisions (Richmond, 2016). The vertical ion velocities, V_{izeE} and V_{izeN}, caused by the eastward ($E_{\perp E}$) and northward ($E_{\perp N}$) perpendicular electric fields are given as (e.g., Chu & Yu, 2017)

$$V_{izeE} = \frac{\cos\theta_D}{1+\xi^2} E_x/B_0 = \frac{\cos\theta_D}{1+\xi^2} E_{\perp E}/B_0 = \frac{1}{1+\xi^2} V_{\perp N}\cos\theta_D \tag{3}$$

$$V_{izeN} = \frac{\xi}{1+\xi^2} E_z/B_0 = \frac{\xi}{1+\xi^2} E_{\perp N}\cos\theta_D/B_0 = -\frac{\xi}{1+\xi^2} V_{\perp E}\cos\theta_D \tag{4}$$

where $V_{\perp N}$ and $V_{\perp E}$ are the F-region ion drift velocities (i.e., the so-called $\vec{E} \times \vec{B}$ velocities) in the northward and eastward directions perpendicular to the geomagnetic field line ($\vec{B}$) as given in Buonsanto et al. (1993) and Buonsanto and Witasse (1999) (see Figures S4 and S5 in Supporting Information S1). As $V_{\perp N}$ is upward from 0 to 6 LT (see Figure 2 in Buonsanto & Witasse, 1999) and ξ increases with decreasing altitude through the E region, the upward V_{izeE} decreases with decreasing altitude, corresponding to divergence of vertical ion velocity. A westward F-region ion velocity $V_{\perp E}$ indicates an upward/poleward electric field $E_{\perp N}$. Such a field produces an upward ion velocity V_{izeN} that maximizes around 125 km where $\xi \approx 1$. Below this height the vertical ion velocity diverges, while above 125 km the velocity converges. The Millstone observations show that the F-region ion velocity is decreasingly westward before dawn (see Figure 3 in Buonsanto & Witasse, 1999).

Adding the effects of Millstone electric fields, which may have magnitudes comparable to those of CTMT winds but quite different phase variations with altitude and time, to the simple model of Figure 3 would change the predicted $TINa^+$ drifts and divergence somewhat. Also, altitude-varying mean winds could affect the $TINa^+$ velocity and convergence. Moreover, tidal components generated in situ are not included in CTMT but could contribute to the $TINa^+$ drift velocity and divergence. The four cases lacking TINa layers are most likely caused by geomagnetic storms that strongly perturb electric fields and/or neutral winds, undermining the TINa formation conditions. It is necessary to develop a TIMt model for midlatitudes to integrate these factors together and quantitatively study the TINa formation mechanisms.

19448007, 2023, 18, Downloaded from https://agupubs.onlinelibrary.wiley.com/doi/10.1029/2023GL105626, Wiley Online Library on [13/09/2023]. See the Terms and Conditions (https://onlinelibrary.wiley.com/terms-and-conditions) on Wiley Online Library for rules of use; OA articles are governed by the applicable Creative Commons License

19448007, 2023, 18, Downloaded from https://agupubs.onlinelibrary.wiley.com/doi/10.1029/2023GL105626, Wiley Online Library on [13/09/2023]. See the Terms and Conditions (https://onlinelibrary.wiley.com/terms-and-conditions) on Wiley Online Library for rules of use; OA articles are governed by the applicable Creative Commons License

Conjugate photoelectrons (CPE) are unimportant on the first-order consideration in predawn TINa formation, because: (a) The conjugate site sunrise is earliest/latest in the Northern Hemisphere winter/summer, opposite to Boulder TINa phase variations. (b) There are not CPE effects in predawn TINa from March–September when conjugate sunrise is later than Boulder local sunrise (see Figures S6 and S7 in Supporting Information S1). (c) In October–February when the conjugate sunrise is earlier, CPE effects are still negligible below 160 km (e.g., Lee et al., 1980a, 1980b; Shepherd et al., 1978; Nagy & Banks, 1970; Richards, 2022).

6. Conclusions

The first characterization of 12 monthly composites of predawn TINa layers using 7 years of lidar data not only unequivocally demonstrates the regular occurrence and phase coherence of these neutral metal layers over Boulder, but also reveals stunning discoveries. The predawn-TINa peak phase time undergoes clear annual variations with the earliest occurrence in summer and latest in winter, which are closely correlated to the annual phase variations of both sunrise and migrating tidal winds in the thermosphere. The predawn TINa neutral layers descend at similar rates as, and in the vertical ion convergence regions, modeled with the migrating tidal winds provided by CTMT, where $TINa^+$ ion accumulation is expected but the tidal vertical wind causes neutrals to diverge. The similarity between descent rates of TINa layers and modeled ion convergence regions supports the formation mechanism, that is, neutralization of converged $TINa^+$ ions forming TINa, proposed in Chu et al. (2021). Phases of migrating tidal winds (SW2 and DW1) in the lower thermosphere experience annual variations, which in turn drive the annual variations of predawn TINa phase. Certainly, the proposed explanation of TINa phase variations and the roles played by various factors need to be verified and quantified with TIMt modeling for midlatitudes. It would be very helpful to have co-located observations of TIMt layers, neutral winds, and ion velocities. Lidar observations of TIMt layers provide a different perspective to study thermal tides in the "thermospheric gap" region of 100–200 km.

Data Availability Statement

The data shown in this work can be downloaded in MatLab data format from Mendeley Data repository (Chen & Chu, 2023, https://data.mendeley.com/datasets/p3k6z9yvmn/3). The Climatological Tidal Model of the Thermosphere (CTMT) data were downloaded from a Clemson University website (https://globaldynamics.sites.clemson.edu/articles/ctmt.html).

Acknowledgments
We are very grateful to Dr. Art Richmond for discussions on TINa/$TINa^+$, to Dr. Jens Oberheide on CTMT tides, and to Dr. Roger Varney on CPEs. We appreciate Wentao Huang, Weichun Fong, John A. Smith, Zhibin Yu, Cao Chen, Zhangjun Wang, Xianxin Li, Chao Chen, Yuli Han, Jian Zhao, and Zhengyu Hua for their contributions to the STAR lidar development, receiver improvement, and/or data collection at Boulder. We offer special thanks to Scott P. Sandberg and Dr. R. Mike Hardesty for their tremendous help in setting up the Table Mountain Lidar Observatory. This work was partially supported by NSF Grants AGS-2330168, OPP-2110428 and AGS-2029162, and NASA solar eclipse funding 80NSSC21K1776.

References

Buonsanto, M. J., Hagan, M. E., Salah, J. E., & Fejer, B. G. (1993). Solar cycle and seasonal variations in F region electrodynamics at Millstone Hill. *Journal of Geophysical Research*, *98*(A9), 15677–15683. https://doi.org/10.1029/93JA01187

Buonsanto, M. J., & Witasse, O. G. (1999). An updated climatology of thermospheric neutral winds and F region ion drifts over Millstone Hill. *Journal of Geophysical Research*, *104*(A11), 24675–24687. https://doi.org/10.1029/1999JA900345

Carter, L. N., & Forbes, J. M. (1999). Global transport and localized layering of metallic ions in the upper atmosphere. *Annales Geophysicae*, *17*(2), 190–209. https://doi.org/10.1007/s005850050750

Chen, Y., & Chu, X. (2023). Lidar observations of predawn thermosphere-ionosphere Na (TINa) layers over Boulder (40.13°N, 105.24°W): Annual phase variations and correlation with sunrise and tidal winds (Version 3) [Dataset]. Mendeley Data. https://data.mendeley.com/datasets/p3k6z9yvmn/3

Chu, X., Chen, Y., Cullens, C. Y., Yu, Z., Xu, Z., Zhang, S., et al. (2021). Mid-latitude thermosphere-ionosphere Na (TINa) layers observed with high-sensitivity Na Doppler Lidar over boulder (40.13°N, 105.24°W). *Geophysical Research Letters*, *48*(11), 1–10. https://doi.org/10.1029/2021GL093729

Chu, X., Nishimura, Y., Xu, Z., Yu, Z., Plane, J. M. C., Gardner, C. S., & Ogawa, Y. (2020). First simultaneous lidar observations of thermosphere-ionosphere Fe and Na (TIFe and TINa) layers at McMurdo (77.84°S, 166.67°E), Antarctica with concurrent measurements of aurora activity, enhanced ionization layers, and converging electric field. *Geophysical Research Letters*, *47*(20), e2020GL090181. https://doi.org/10.1029/2020GL090181

Chu, X., & Yu, Z. (2017). Formation mechanisms of neutral Fe layers in the thermosphere at Antarctica studied with a thermosphere-ionosphere Fe/Fe^+ (TIFe) model. *Journal of Geophysical Research: Space Physics*, *122*(6), 6812–6848. https://doi.org/10.1002/2016JA023773

Chu, X., Yu, Z., Gardner, C. S., Chen, C., & Fong, W. (2011). Lidar observations of neutral Fe layers and fast gravity waves in the thermosphere (110-155 km) at McMurdo (77.8°S, 166.7°E), Antarctica. *Geophysical Research Letters*, *38*(23), 1–6. https://doi.org/10.1029/2011GL050016

Cullens, C. Y., Immel, T. J., Triplett, C. C., Wu, Y. J., England, S. L., Forbes, J. M., & Liu, G. (2020). Sensitivity study for ICON tidal analysis. *Progress in Earth and Planetary Science*, *7*(1), 18. https://doi.org/10.1186/s40645-020-00330-6

Forbes, J. M., Oberheide, J., Zhang, X., Cullens, C., Englert, C. R., Harding, B. J., et al. (2022). Vertical coupling by solar semidiurnal tides in the thermosphere from ICON/MIGHTI measurements. *Journal of Geophysical Research: Space Physics*, *127*(5), 1–33. https://doi.org/10.1029/2022JA030288

Friedman, J. S., Chu, X., Brum, C., & Lu, X. (2013). Observation of a thermospheric descending layer of neutral K over Arecibo. *Journal of Atmospheric and Solar-Terrestrial Physics*, *104*, 253–259. https://doi.org/10.1016/j.jastp.2013.03.002

Gao, Q., Chu, X., Xue, X., Dou, X., Chen, T., & Chen, J. (2015). Lidar observations of thermospheric Na layers up to 170 km with a descending tidal phase at Lijiang (26.7°N, 100.0°E), China. *Journal of Geophysical Research: Space Physics*, *120*(10), 9213–9220. https://doi.org/10.1002/2015JA021808

Immel, T. J., England, S. L., Mende, S. B., Heelis, R. A., Englert, C. R., Edelstein, J., et al. (2018). The ionospheric connection explorer mission: Mission goals and design. *Space Science Reviews*, *214*(1), 13. https://doi.org/10.1007/s11214-017-0449-2

Jiao, J., Chu, X., Jin, H., Wang, Z., Xun, Y., Du, L., et al. (2022). First Lidar profiling of meteoric Ca+ ion transport from ∼80 to 300 km in the midlatitude nighttime ionosphere. *Geophysical Research Letters*, *49*(18), e2022GL100537. https://doi.org/10.1029/2022gl100537

Kopp, E. (1997). On the abundance of metal ions in the lower ionosphere. *Journal of Geophysical Research*, *102*(A5), 9667–9674. https://doi.org/10.1029/97JA00384

Lee, J. S., Doering, J. P., Potemra, T. A., & Brace, L. H. (1980a). Measurements of the ambient photoelectron spectrum from atmosphere explorer: I. AE-E measurements below 300 km during solar minimum conditions. *Planetary and Space Science*, *28*(10), 947–971. https://doi.org/10.1016/0032-0633(80)90058-6

Lee, J. S., Doering, J. P., Potemra, T. A., & Brace, L. H. (1980b). Measurements of the ambient photoelectron spectrum from atmosphere explorer: II. AE-E measurements from 300 to 1000 km during solar minimum conditions. *Planetary and Space Science*, *28*(10), 973–996. https://doi.org/10.1016/0032-0633(80)90059-8

Liu, A. Z., Guo, Y., Vargas, F., & Swenson, G. R. (2016). First measurement of horizontal wind and temperature in the lower thermosphere (105–140 km) with a Na Lidar at Andes Lidar Observatory. *Geophysical Research Letters*, *43*(6), 2374–2380. https://doi.org/10.1002/2016GL068461

Lübken, F. J., Höffner, J., Viehl, T. P., Kaifler, B., & Morris, R. J. (2011). First measurements of thermal tides in the summer mesopause region at Antarctic latitudes. *Geophysical Research Letters*, *38*(24), L24806. https://doi.org/10.1029/2011GL050045

Nagy, A. F., & Banks, P. M. (1970). Photoelectron fluxes in the ionosphere. *Journal of Geophysical Research*, *75*(31), 6260–6270. https://doi.org/10.1029/ja075i031p06260

Oberheide, J. (2022). Day-to-day variability of the semidiurnal tide in the F-region ionosphere during the January 2021 SSW from COSMIC-2 and ICON. *Geophysical Research Letters*, *49*(17), e2022GL100369. https://doi.org/10.1029/2022GL100369

Oberheide, J., Forbes, J. M., Zhang, X., & Bruinsma, S. L. (2011). Climatology of upward propagating diurnal and semidiurnal tides in the thermosphere. *Journal of Geophysical Research*, *116*(A11), A11306. https://doi.org/10.1029/2011JA016784

Picone, J. M., Hedin, A. E., Drob, D. P., & Aikin, A. C. (2002). NRLMSISE-00 empirical model of the atmosphere: Statistical comparisons and scientific issues. *Journal of Geophysical Research*, *107*(A12), 1–16. https://doi.org/10.1029/2002JA009430

Plane, J. M. C. (2003). Atmospheric chemistry of meteoric metals. *Chemical Reviews*, *103*(12), 4963–4984. https://doi.org/10.1021/cr0205309

Plane, J. M. C., Feng, W., & Dawkins, E. C. M. (2015). The mesosphere and metals: Chemistry and changes. *Chemical Reviews*, *115*(10), 4497–4541. https://doi.org/10.1021/cr500501m

Raizada, S., Brum, C. M., Tepley, C. A., Lautenbach, J., Friedman, J. S., Mathews, J. D., et al. (2015). First simultaneous measurements of Na and K thermospheric layers along with TILs from Arecibo. *Geophysical Research Letters*, *42*(23), 10106–10112. https://doi.org/10.1002/2015GL066714

Raizada, S., Smith, J. A., Lautenbach, J., Aponte, N., Perillat, P., Sulzer, M., & Mathews, J. D. (2020). New lidar observations of Ca+ in the mesosphere and lower thermosphere over arecibo. *Geophysical Research Letters*, *47*(5), 1–9. https://doi.org/10.1029/2020GL087113

Richards, P. G. (2022). Ionospheric photoelectrons: A lateral thinking approach. *Frontiers in Astronomy and Space Sciences*, *9*, 1–6. https://doi.org/10.3389/fspas.2022.952226

Richmond, A. D. (2016). Ionospheric electrodynamics. In G. V. Khazanov (Ed.), *Space weather fundamentals, chapter 14* (pp. 245–259). CRC Press. https://doi.org/10.1201/9781315368474

Shepherd, G. G., Pieau, J. F., Ogawa, T., Tohmatsu, T., Oyama, K., & Watanabe, Y. (1978). Direct measurement of conjugate photoelectrons and predawn 630 nm airglow. *Planetary and Space Science*, *26*(3), 211–217. https://doi.org/10.1016/0032-0633(78)90086-7

Shinagawa, H., Miyoshi, Y., Jin, H., & Fujiwara, H. (2017). Global distribution of neutral wind shear associated with sporadic E layers derived from GAIA. *Journal of Geophysical Research: Space Physics*, *122*(4), 4450–4465. https://doi.org/10.1002/2016JA023778

Smith, J. A., & Chu, X. (2015). High-efficiency receiver architecture for resonance-fluorescence and Doppler lidars. *Applied Optics*, *54*(11), 3173–3184. https://doi.org/10.1364/AO.54.003173

Tsuda, T. T., Chu, X., Nakamura, T., Ejiri, M. K., Kawahara, T. D., Yukimatu, A. S., & Hosokawa, K. (2015). A thermospheric Na layer event observed up to 140 km over Syowa Station (69.0°S, 39.6°E) in Antarctica. *Geophysical Research Letters*, *42*(10), 3647–3653. https://doi.org/10.1002/2015GL064101

Verner, D. A., & Ferland, G. J. (1996). Atomic data for astrophysics: I. Radiative recombination rates for H-like, He-like, Li-like, and Na-like ions over a broad range of temperature. *Astrophysical Journal Supplement*, *103*, 467. https://doi.org/10.1086/192284

Wang, J., Yang, Y., Cheng, X., Yang, G., Song, S., & Gong, S. (2012). Double sodium layers observation over Beijing, China. *Geophysical Research Letters*, *39*(15), L15801. https://doi.org/10.1029/2012GL052134

Wu, F., Chu, X., Du, L., Jiao, J., Zheng, H., Xun, Y., et al. (2022). First simultaneous Lidar observations of thermosphere-ionosphere sporadic Ni and Na (TISNi and TISNa) Layers (∼105–120 km) Over Beijing (40.42°N, 116.02°E). *Geophysical Research Letters*, *49*(16), e2022GL100397. https://doi.org/10.1029/2022gl100397

Xun, Y., Yang, G., She, C.-Y., Wang, J., Du, L., Yan, Z., et al. (2019). The first concurrent observations of thermospheric Na layers from two nearby central midlatitude Lidar stations. *Geophysical Research Letters*, *46*(4), 1892–1899. https://doi.org/10.1029/2018GL081645

Yu, Z., Chu, X., Huang, W., Fong, W., & Roberts, B. R. (2012). Diurnal variations of the Fe layer in the mesosphere and lower thermosphere: Four season variability and solar effects on the layer bottomside at McMurdo (77.8S, 166.7E), Antarctica. *Journal of Geophysical Research*, *117*(22), 1–15. https://doi.org/10.1029/2012JD018079

19448007, 2023, 18, Downloaded from https://agupubs.onlinelibrary.wiley.com/doi/10.1029/2023GL105626, Wiley Online Library on [13/09/2023]. See the Terms and Conditions (https://onlinelibrary.wiley.com/terms-and-conditions) on Wiley Online Library for rules of use; OA articles are governed by the applicable Creative Commons License